Supplementary Information

Porphyrin Metal-Organic Frameworks with Bilayer and Pillar-layered Frameworks for Third-order Nonlinear Optical Properties

Ziyi Zhu[a], Zirui Wang[a,b], Qiao-Hong Li[a], Zhizhou Ma[a], Fei Wang[a]*, and Jian Zhang[a]*

[a] State Key Laboratory of Structural Chemistry, Fujian Institute of Research on the Structure of Matter, the Chinese Academy of Sciences, Fuzhou, Fujian 350002, People's Republic of China.

[b] School of Physical Science and Technology, ShanghaiTech University, Shanghai 201210, China. E-mail: wangfei04@fjirsm.ac.cn.

1. Experimental Section

The S,S-BED was synthesized according to our former work. All other chemicals were commercially purchased and directly used without further purification. Fourier transform infrared (FT-IR) spectra were recorded with a Spectrum One FT-IR Spectrometer in the 400-4000 cm-1 range. Thermogravimetric analysis (TGA) data were carried out in an N2 atmosphere with a heating rate of 10 °C/min on a STA 449F3 integration thermal analyzer. The UV-Vis (UV) absorption spectra data were carried out using Lambda-950 UV-Vis spectrophotometer. Powder X-ray diffraction (PXRD) data were collected on a Rigaku Mini Flex II diffractometer using CuKα radiation (λ = 1.54056 Å) in the 2θ range of 5-50° with a scanning rate of 10° min-1. The AFM images were recorded with a Bruker Dimension ICON. X-ray photoelectron spectroscopy (XPS) spectra for the samples were recorded by using an ESCALAB250Xi. Transmission electron microscope (TEM) images recorded for the samples were used JEM-2010F.

1.1 Synthesis of OH-opd

Synthesis of OH-opd: 10.8 g, 0.1 mol of o-phenylenediamine, 8.0 g, 0.054 mol of L-malic acid and 4 mol/L, 100 ml of hydrochloric acid were mixed in a round bottom flask at room temperature and stirred for about 5 minutes, then heated to reflux in an oil bath at 115°C for 9 hours. The reaction was dark green, and after standing overnight,

the green protonated chloride crystalline salt was formed, filtered until drained, and the precipitate was filtered out into a 500 mL round bottom flask with 100 mL of water and 0.3 g of activated carbon (heated to 100°C for complete dissolution), refluxed for two hours, filtered while hot, and the filtrate was removed and adjusted to pH 8-9 with aqueous sodium hydroxide, filtered, washed and dried to obtain the sample (yield: 45%, Calculation based on o-phenylenediamine).[1]

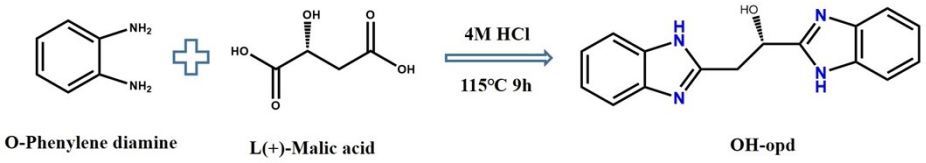

O-Phenylene diamine L(+)-Malic acid OH-opd

Scheme S1. The synthesis of OH-opd ligands

1.2 Synthesis of PMOF-1

$Zn(NO_3)_2 \cdot 6H_2O$ (80.0 mg, 0.42 mmol), S,S-BED (60 mg, 0.2 mmol) and tetracarboxyphenylporphyrin (TCPP, 50.0 mg, 0.063 mmol) dissolved in a mixed solvent of 3 mL DEF, 2 mL 1,4-Dioxane and 2 mL H_2O were placed in a 20 mL vial. The sample was then heated at 100 °C for 6 days and then cooled to room temperature. After washing with ethanol, red crystals were obtained (yield about 34.0 % based on TCPP).

1.3 Synthesis of PMOF-2

$Zn(NO_3)_2 \cdot 6H_2O$ (80.0 mg, 0.42 mmol), S,S-BED (60 mg, 0.2 mmol) and tetracarboxyphenylporphyrin (TCPP, 50.0 mg, 0.063 mmol) dissolved in a mixed solvent of 3 mL DMF, 2 mL 1,4-Dioxane and 2 mL H_2O were placed in a 20 mL vial. The sample was then heated at 100 °C for 5 days and then cooled to room temperature. After washing with Stock solution, red crystals were obtained (yield about 31.0 % based on TCPP).

1.4 Prepare of MOFs dispersed PDMS

PDMS glass were fabricated using Sylgard 184 (Dow Corning) by thoroughly mixing 10 parts base to part curing agent. The MOFs crystals were stripped into MOFs nanoblock and were mixed with the PDMS solution to form MOFs dispersed PDMS suspension. And then, the mixture suspension was added into a template and then put

the template into a vacuum oven at 60 °C for 5 hours. Last, the transparant and flexible MOFs/PDMS glasses were obtained.[2]

1.5 Z-scan measurements

The nonlinear optical properties of the PMOFs were evaluated using the Z-scan technique. The excitation light source was an Nd:YAG laser with a repetition rate of 5 Hz. The laser pulses (period, 5 ns; wavelength, 532 nm) were split into two beams with a mirror. The pulse energies at the front and back of the samples were monitored using energy detectors 1 and 2. All of the measurements were conducted at room temperature. The sample was mounted on a computer-controlled translation stage that shifted each sample along the Z-axis.

1.6 Calculation of the nonlinear optical parameters

The imaginary parts of the third-order susceptibility (*Im* $\chi^{(3)}$) and the real parts of third-order susceptibility (*Re* $\chi^{(3)}$) were determined through relations:

$$lm\chi^{(3)}(esu) = \frac{c^2 n_0^2 \beta \left(m/W\right)}{240\pi^2 \omega}$$

$$Re\chi^{(3)}(esu) = \frac{c n_0^2 n_2 \left(m^2/W\right)}{120\pi^2}$$

Where ω is angular frequency of the incident wavelength, β is the nonlinear absorption coefficient, n_2 is the nonlinear refractive index parameter, c is the speed of light in vacuum, λ is the wavelength of the laser pulse and n_0 is the linear refractive index, respectively.

The absolute value of the third-order NLO susceptibility ($\chi^{(3)}$) of the ZnTCPP were determined according to the following relations:

$$|\chi^{(3)}| = \sqrt{|lm\chi^{(3)}|^2 + |lm\chi^{(3)}|^2}$$

The relationship of the sample transmission and input laser intensity for a spatially Gaussian beam could be plotted from the open-aperture Z-scan curve. From the input

laser pulse energy E_{in} and beam radius $\omega(z)$, the light fluence $F_{in}(z)$ at any position could be obtained. $F_{in}(z)$ was defined as:

$$F_{in}(z) = \frac{4E_{in}\sqrt{ln2}}{\pi^{\frac{3}{2}}\omega(z)^2}$$

Where ω(z) was defined as:

$$\omega(Z) = \frac{\omega_0}{\left[1 + \left(\frac{z}{z_0}\right)^2\right]^{-0.5}}$$

where ω_0 and z_0 are the light beam radius and the Rayleigh range, respectively, and z_0 was defined as:

$$z_0 = \frac{k\omega_0^2}{2}$$

Where k was defined as:

$$k = \frac{2\pi}{\lambda}$$

The curve of output fluence versus input fluence in Figure 4(b) was plotted from Figure 4(c).

The equation fits for the nonlinear adsorption coefficient β as follows:

$$T(Z, S = 1) = \frac{1}{\pi^{\frac{1}{2}}(Z, 0)} \int_{-\infty}^{\infty} \ln\left[1 + q_0(Z, 0)e^{-r^2}\right] dr$$

$$q_0(Z, 0) = \beta I_0 L_{eff}$$

$$L_{eff} = \frac{1 - e^{-\alpha l}}{\alpha}$$

In these equations, I_0 is the on-axis peak intensity at the focus (Z = 0), L_{eff} is the effective thickness of the sample, α is the linear absorption coefficient, and l is the sample thickness.

1.7 Photocurrent measurement

We prepared the working electrode by solution coating method as follows: the newly prepared sample (5 mg) and Nafion (10 μL) dissolved in 0.5 mL ethanol with ultrasound and 40 μL solution was uniformly dropped on clean FTO conductive glass (1.0 × 4.0 cm^2, 10 Ω·cm^{-2}). The photocurrent experiment was carried out on the CHI760E electrochemical workstation of the three electrode system, in which Pt sheet was the counter electrode and Ag/AgCl electrode was the reference electrode. The experiment was carried out in 0.2 M Na_2SO_4 electrolyte at room temperature, and a 300 W high-pressure xenon lamp (full band) was used as a visible light source.

2. Single crystal synthesis and characterization of compound

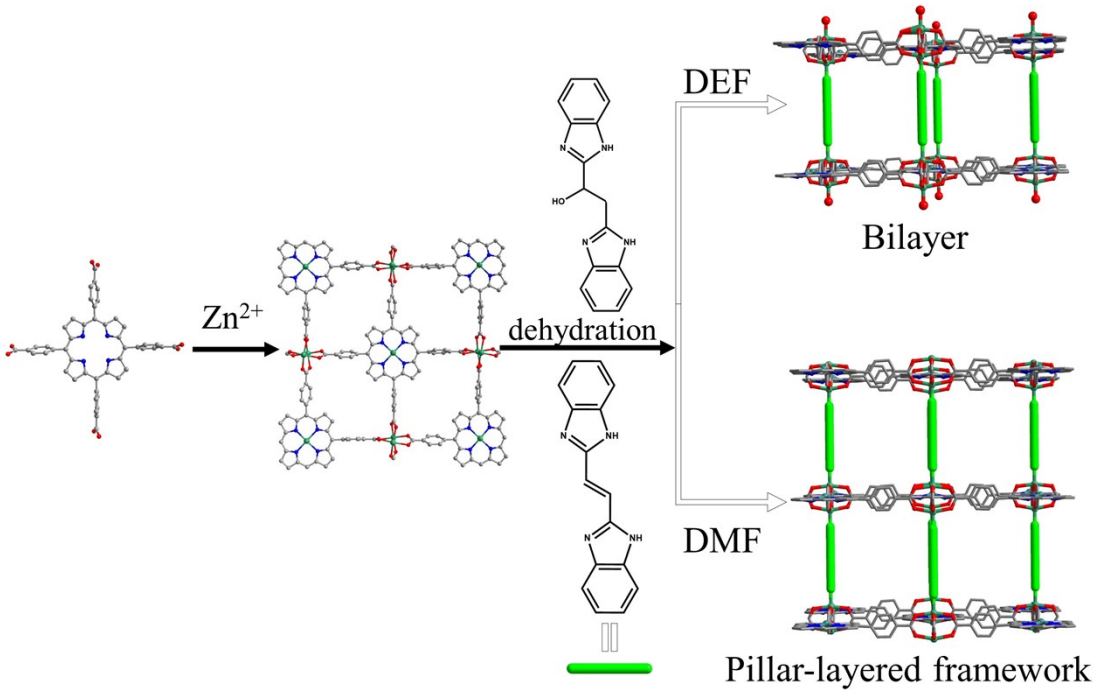

Scheme S2. Illustration of the synthesis for **PMOF-1** and **PMOF-2**.

Table S1. Crystallographic data and structure refinement for **PMOF-1** and **PMOF-2**.

Identification code	PMOF-1	PMOF-1
Empirical formula	$C_{64}H_{48}N_6O_{13}Zn_3$	$C_{64}H_{34}N_8O_8Zn_3$
Formula weight	1304.18	1239.1
Temperature/K	100.0(13)	100.0(13)
Crystal system	triclinic	monoclinic
Space group	*P*-1	*C*2/*c*
a/Å	16.6123(5)	23.5128(4)
b/Å	16.6936(6)	23.5272(3)
c/Å	16.7212(6)	18.2894(3)
α/°	118.127(4)	90
β/°	90.188(3)	96.728(2)
γ/°	108.145(3)	90
Volume/Å^3	3823.3(3)	10047.8(3)
Z	2	4
ρ_{calc}g/cm^3	1.133	0.819
μ/mm^{-1}	1.551	0.743
F(000)	1334	2512
Crystal size/mm^3	0.1 × 0.1 × 0.1	0.1 × 0.1 × 0.1
Goodness-of-fit on F^2	1.051	1.055
Final R indexes [I>=2σ (I)]	R_1 = 0.0555, wR_2 = 0.1612	R_1 = 0.0815, wR_2 = 0.2274
Final R indexes [all data]	R_1 = 0.0639, wR_2 = 0.1677	R_1 = 0.0872, wR_2 = 0.2327
CCDC	2235076	2235077

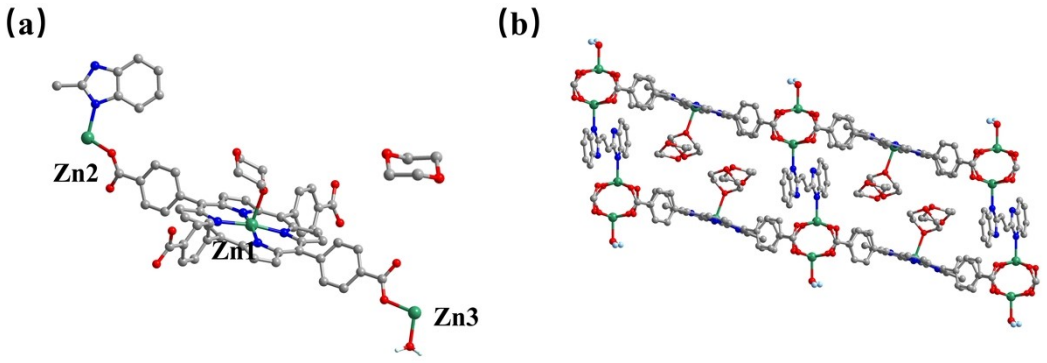

Figure S1. (a) the asymmetric unit of PMOF-1; (b) view of the 2D bilayer of PMOF-1 containing coordinated 1,4-Dioxane and guest 1,4-Dioxane.

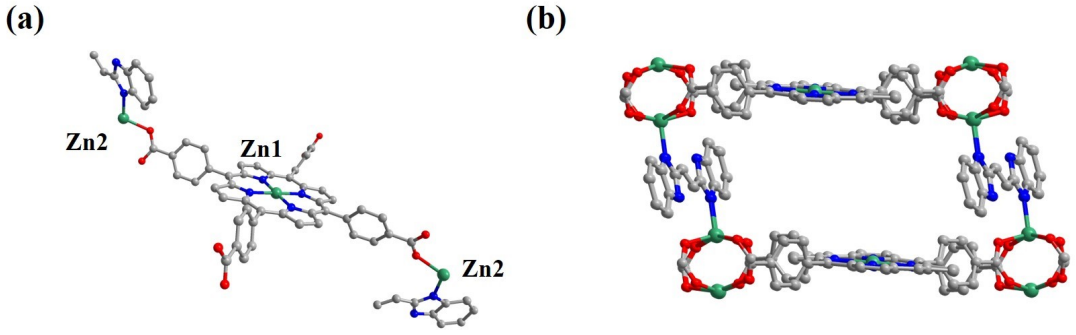

Figure S2. (a) the asymmetric unit of PMOF-2; (b) Pore size of PMOF-2.

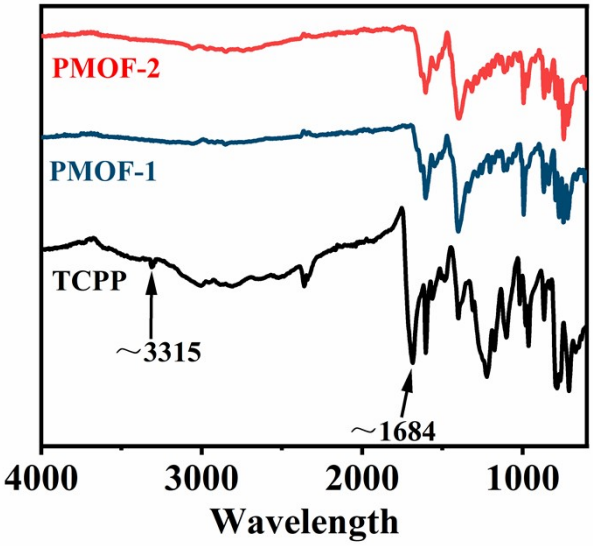

Figure S3. The IR spectra of **PMOF-1**, **PMOF-2** and TCPP.

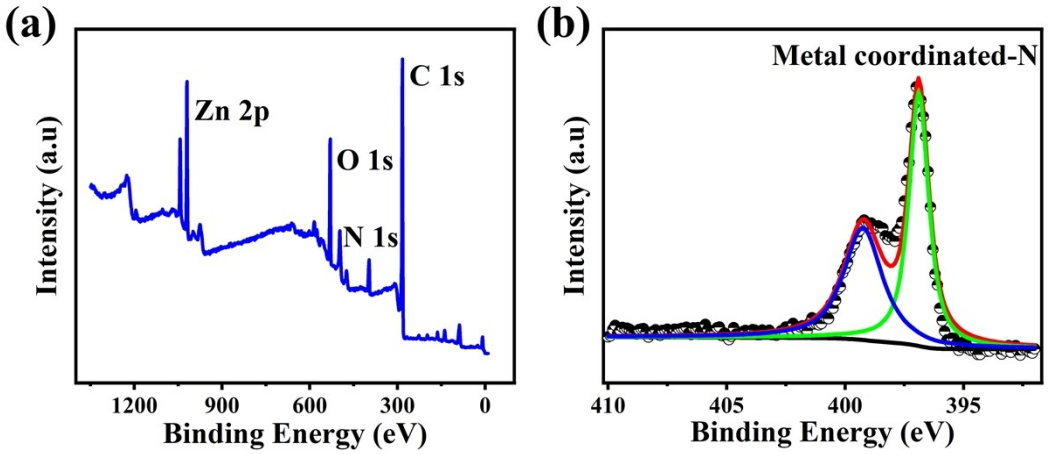

Figure S4. (a) The survey XPS and (b) N 1s XPS spectra of **PMOF-1**.

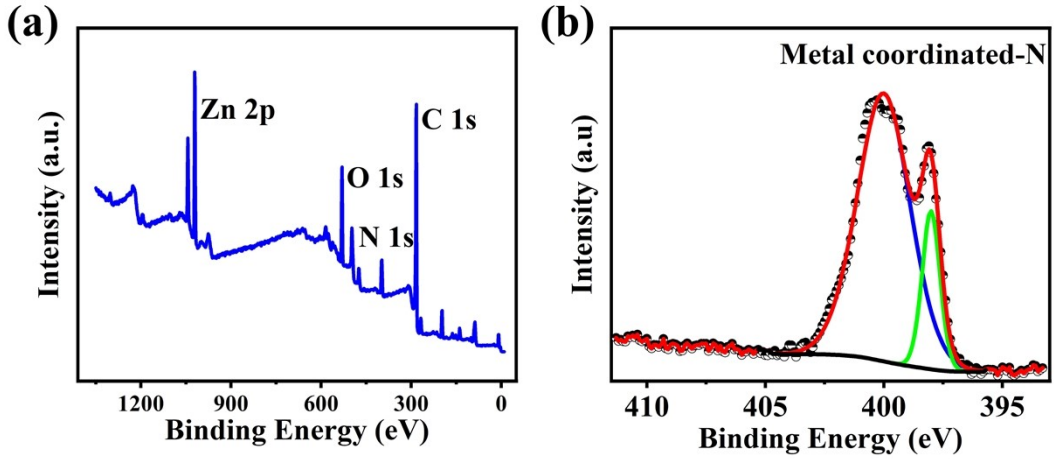

Figure S5. (a) The survey XPS and (b) N 1s XPS spectra of **PMOF-2**.

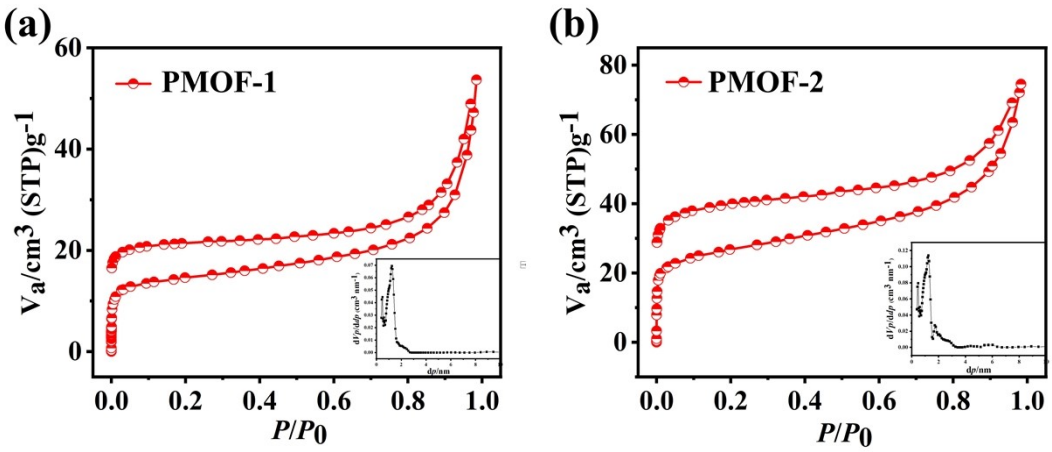

Figure S6. The Adsorption of **PMOF-1**, **PMOF-2**.

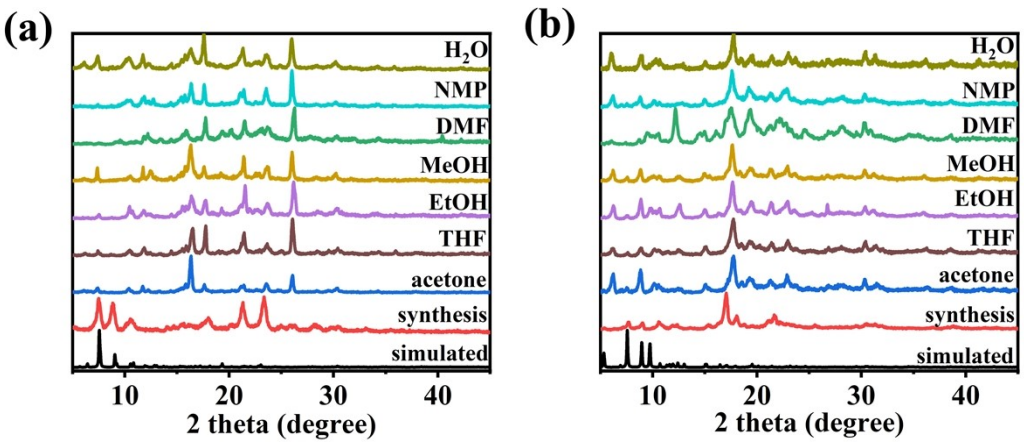

Figure S7. The stability of PMOF-1 (a) and PMOF-2 (b) in different solvents at room temperature.

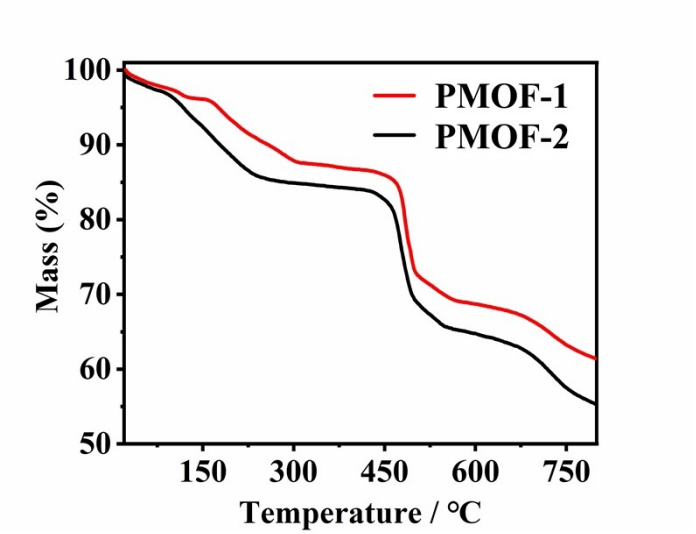

Figure S8. The TG of **PMOF-1**, **PMOF-2**.

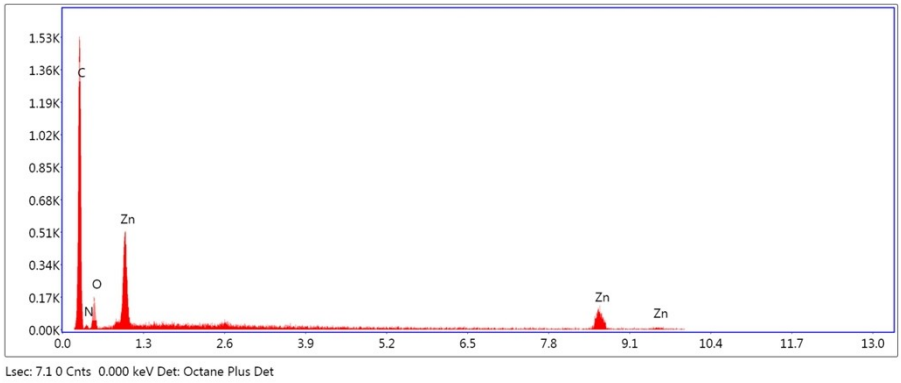

Figure S9. The SEM EDS of **PMOF-1**.

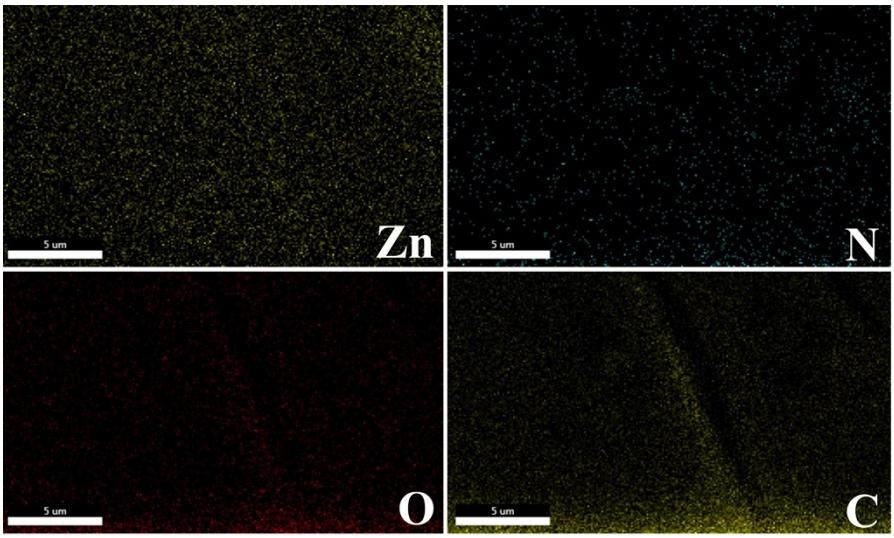

Figure S10. The SEM elemental mapping of **PMOF-1**.

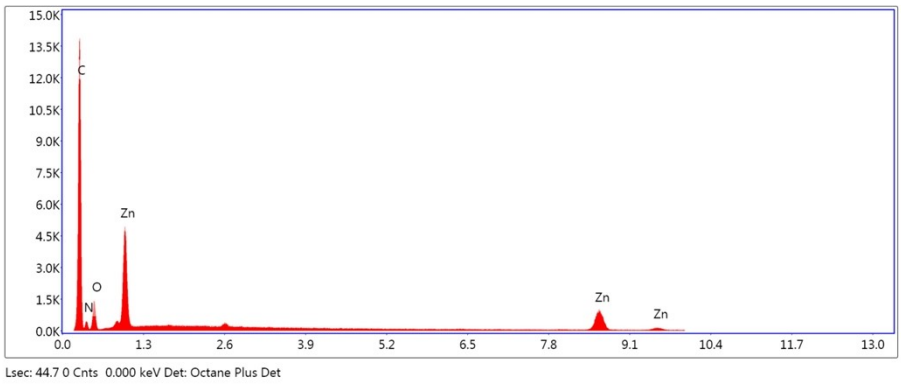

Figure S11. The SEM EDS of **PMOF-2**.

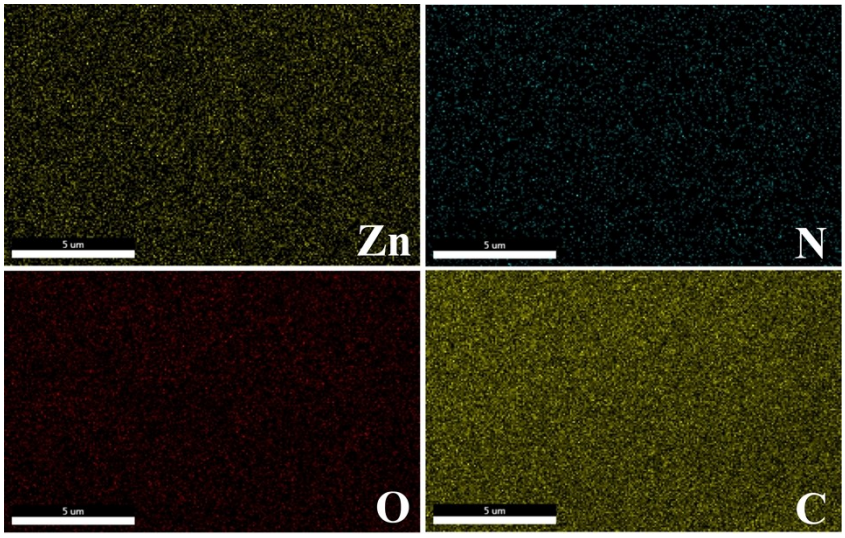

Figure S12. The SEM elemental mapping of **PMOF-2.**

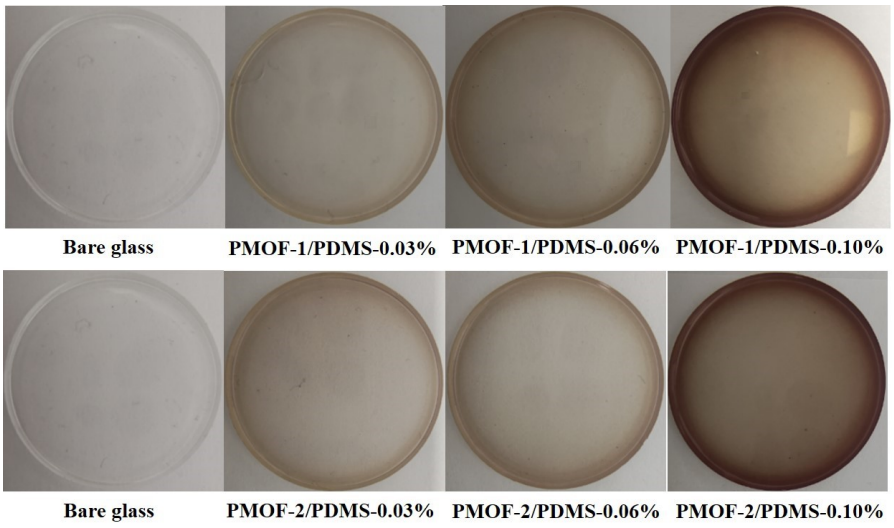

Figure S13. The photograph of **PMOF-1/PDMS** and **PMOF-2/PDMS** with different concentrations.

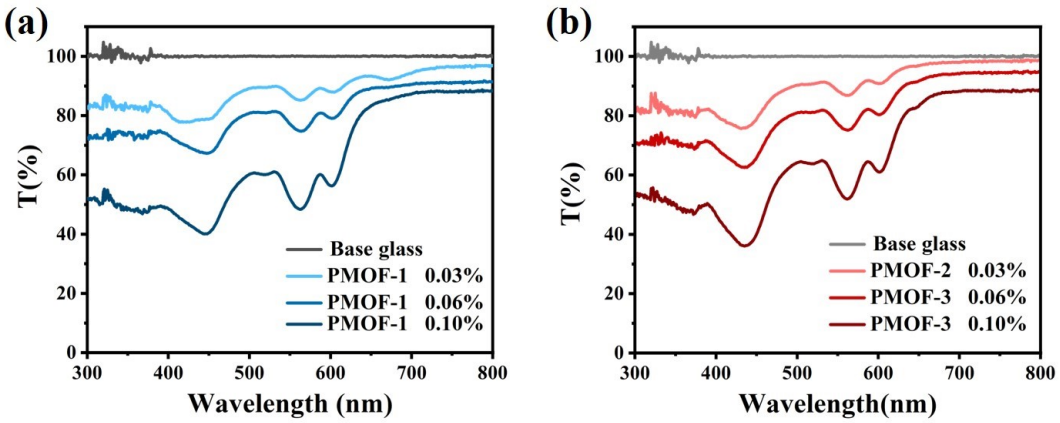

Figure S14. The linear transmittances of **PMOF-1/PDMS** and **PMOF-2/PDMS** with different concentrations.

3. Third order nonlinear optical measurement

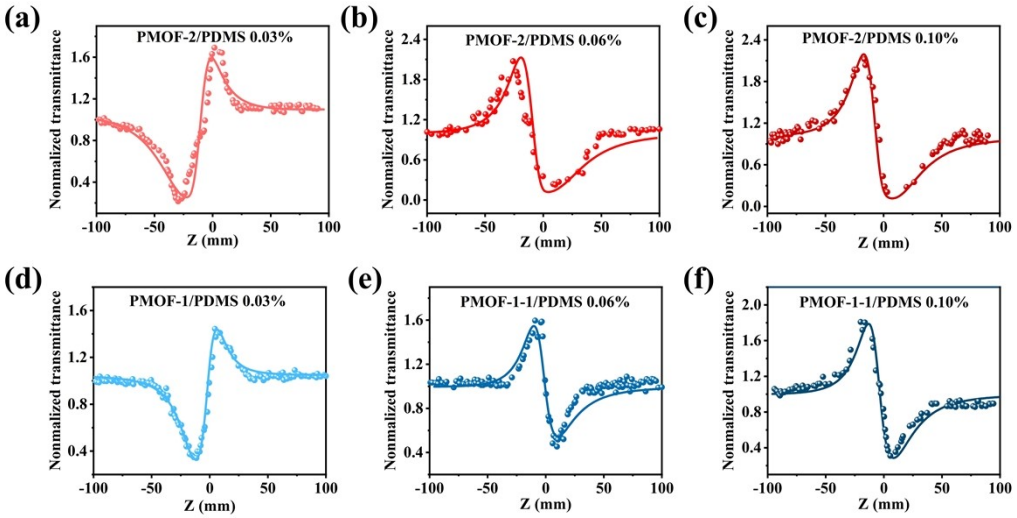

Figure S15. Nonlinear refractive response of **PMOF/PDMS** showed a clear peak-to-trough trend, indicating their self-defocusing behavior.

Table S2. The comparison of the nonlinear absorption coefficients.

Samples	**Nonlinear absorption coefficient (cm/GW)**	**References**
PMOF-2/PDMS	**1165**	**This work**
PMOF-1/PDMS	**625**	**This work**
ZnTPyP-1(Zn/Cu)/PDMS	4650	[2]
Por-COF-ZnCu	4470	[3]

Por-COF-ZnNi	4170	
Por-COF-HH	1170	
Por-TzTz-POF	1100	[4]
MQD-TPP/PMMA film	1059.2	[5]
Pure grapheme	900	[6]
Zinc porphyrin	366	
Copper porphyrin	132	
$[(TBA)_8\{(4\text{-}TPP\text{-}Mn)(Mo_6O_{18})_4]$	98	[7]
$Si(OH)_2TPPc$	136	[8]
DNDs-$Si(OH)_2TPPc$	125	
DNDs-ZnTPPc	60.9	
DNDs-H_2TPPc	58.5	
ZnTPPc	42.8	
H_2TPPc	41	
P_2Pt	45	[9]
P_1Pt	39	
1-GO	93	[10]
GO	2.6	
PIZA-1	28	[11]
C_{60}@PIZA-1	19	
HKUST-1-200	1.6	[12]

Table S3. Linear and NLO data of **PMOF-1/PDMS** with different concentrations.

Samples	**Tmin**	**β (×10^{-9}m/W)**	**Im χ $^{(3)}$ (×10^{-11} esu)**	**F_{OL} (J cm^{-1})**
0.03%	**0.92**	**3.60**	**7.35**	**1.74**
0.06%	**0.84**	**5.05**	**11.6**	**0.97**
0.10%	**0.50**	**6.25**	**12.3**	**0.60**

Note: Tmin: Transmissivity; ***β***: nonlinear coefficient; ***Im*** $\chi^{(3)}$: the imaginary parts of the third-order susceptibility; F_{OL}**:** limiting threshold.

Table S4. Linear and NLO data of **PMOF-2/PDMS** with different concentrations.

Samples	Tmin	β (×10^{-9}m/W)	Im χ $^{(3)}$ (×10^{-11} esu)	F_{OL} (J cm^{-1})
0.03%	0.87	5.45	11.4	1.40
0.06%	0.74	9.25	20.3	0.54
0.10%	0.43	11.65	24.1	0.24

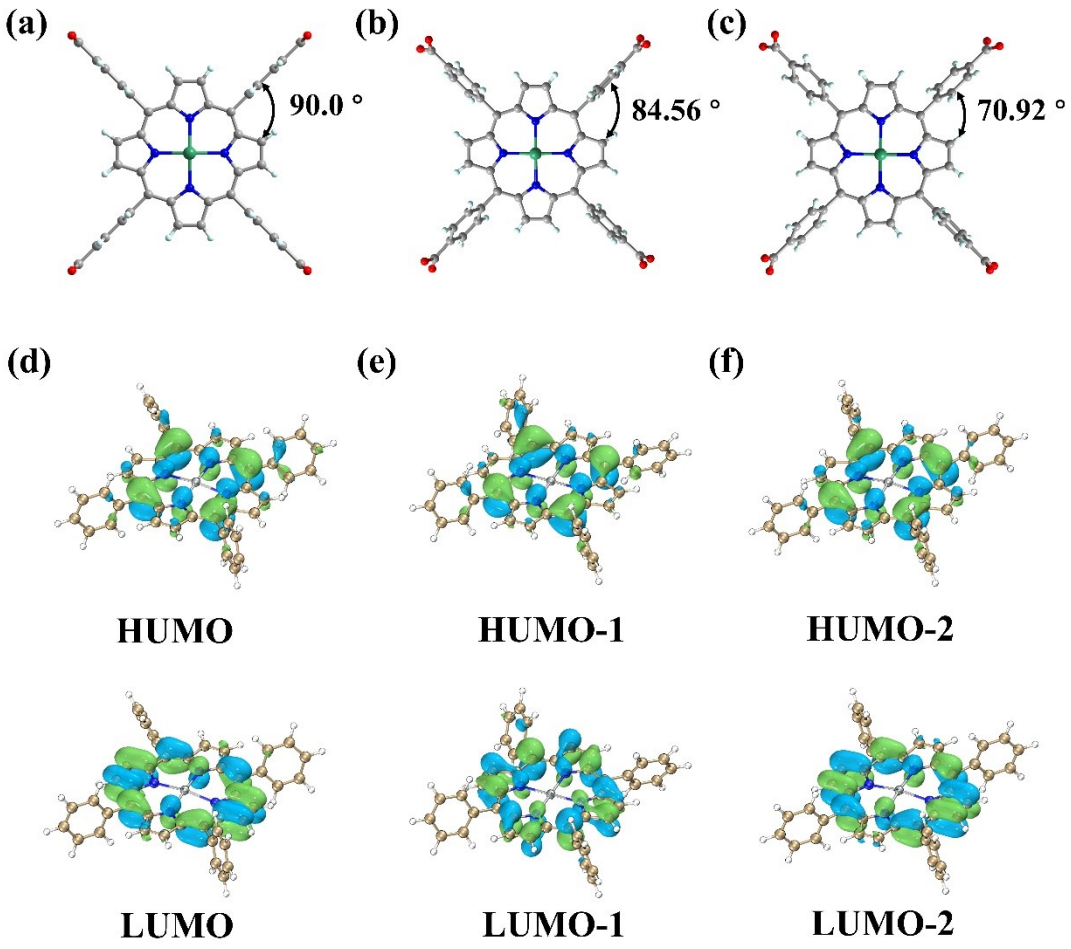

Figure S16. The frontier molecular orbitals diagram of HOMO and LUMO for PMOF-1 and PMOF-2 are compared with Zn-TCPP 2D.

To gain further insight into NLO performance of dimension in PMOFs, the theoretical calculation based on DFT was performed, and the noninterpenetrated Part A and Part B For the PMOF structures. when the angle between porphyrin ring and benzene is 70.92°, it is more stable than 84.56° (△E=0.078 eV), and 90° (△E=0.470

eV). The highest occupied molecular orbital (HOMO) and lowest unoccupied molecular orbital (LUMO) are mainly distributed on the porphyrin ring, and the HOMO-LUMO gap of PMOF-2 (70.92°) is 0.0044 eV and 0.0255 eV smaller than that of PMOF-1 (84.56°) and Zn-TCPP (90°), respectively. From the perspective of charge transfer, the three ZnTCPP structures are mainly electron redistribution within the porphyrin ring (Zn-TCPP (90°): 94.18%, PMOF-1 (84.56°): 93.73%, PMOF-2 (70.92°): 93.53%), but with the decrease of angle, the charge transfer amount between porphyrin and benzene ring increases (Zn-TCPP (90°): 5.73%, PMOF-1 (84.56°): 6.17%, PMOF-2 (70.92°): 6.37%), this makes PMOF-2 have more excellent third-order performance.

Reference

1. Z.-W. Wang, Z.-Y. Zhu, S. Li and F. Wang, *CrystEngComm*, 2022, **24**, 3465-3468.
2. D. J. Li, Q. H. Li, Z. R. Wang, Z. Z. Ma, Z. G. Gu and J. Zhang, *J Am Chem Soc*, 2021, **143**, 17162-17169.
3. B. P. Biswal, S. Valligatla, M. Wang, T. Banerjee, N. A. Saad, B. M. K. Mariserla, N. Chandrasekhar, D. Becker, M. Addicoat, I. Senkovska, R. Berger, D. N. Rao, S. Kaskel and X. Feng, *Angew Chem Int Ed Engl*, 2019, **58**, 6896-6900.
4. M. Samal, S. Valligatla, N. A. Saad, M. V. Rao, D. N. Rao, R. Sahu and B. P. Biswal, *Chem Commun (Camb)*, 2019, **55**, 11025-11028.
5. P. Jiang, B. Zhang, Z. Liu and Y. Chen, *Nanoscale*, 2019, **11**, 20449-20455.
6. N. Jia, C. He, S. Wang, W. Song, Z. Chen, Y. Zu, Y. Gao and Y. Dong, *Optical Materials*, 2018, **76**, 81-89.
7. S. u. Hassan, F. Nawaz, Z. U. Haq Khan, A. Firdous, M. A. Farid and M. S. Nazir, *Optical Materials*, 2018, **86**, 106-112.
8. R. Matshitse, S. Khene and T. Nyokong, *Diamond and Related Materials*, 2019, **94**, 218-232.
9. Z. Liu, J. Sun, C. Yan, Z. Xie, G. Zhang, X. Shao, D. Zhang and S. Zhou, *Journal of Materials Chemistry C*, 2020, **8**, 12993-13000.
10. K. Garg, R. Shanmugam and P. C. Ramamurthy, *Carbon*, 2017, **122**, 307-318.
11. D. J. Li, Z. G. Gu and J. Zhang, *Chem Sci*, 2020, **11**, 1935-1942.
12. Z. G. Gu, D. J. Li, C. Zheng, Y. Kang, C. Woll and J. Zhang, *Angew Chem Int Ed Engl*, 2017, **56**, 6853-6858.